

Manipulating nonadiabatic dynamics by plasmonic nanocavity

Yu Wang,^{†,‡} Ruihao Bi,^{†,‡} and Wenjie Dou^{*,†,‡}

[†]*Department of Chemistry, School of Science, Westlake University, Hangzhou 310024
Zhejiang, China*

[‡]*Institute of Natural Sciences, Westlake Institute for Advanced Study, Hangzhou 310024
Zhejiang, China*

E-mail: douwenjie@westlake.edu.cn

Abstract

In recent years, plasmonic nanocavities have emerged as powerful tools for controlling and enhancing light-matter interactions at the nanoscale. This study explores the role of plasmonic nanocavities in manipulating nonadiabatic dynamics, particularly in systems where fast electronic transitions are crucial. By coupling molecular states to the plasmonic resonances of metallic nanocavities, we demonstrate that the local electromagnetic fields generated by plasmons can significantly influence the rates and pathways of nonadiabatic transitions, including electron transfer and excitation relaxation processes. Using the Floquet quantum master equation (FQME) and Floquet surface hopping (FSH) methods that we previously developed, we find that plasmonic nanocavities can enhance nonadiabatic effects by tuning the plasmonic coupling strength, the molecule-metal interaction strength, and the material properties. These approaches offer a new perspective for predicting molecular dynamics in ultrafast processes. Our findings pave the way for designing novel plasmonic devices capable of

controlling electron and energy transfer in chemical reactions, optoelectronic applications, and quantum information processing.

1. INTRODUCTION

A plasmonic nanocavity is a nanoscale structure that supports surface plasmon polaritons (SPPs)—oscillations of free electrons in a metal coupled with electromagnetic fields. These cavities can confine light to subwavelength scales, enhancing local electromagnetic fields.^{1–4} Plasmonic nanocavities, such as metallic nanoparticles or sharp tips in gap structures, exhibit field enhancement at metal-dielectric interfaces or in nanoscale gaps.^{5–8} Plasmonic volumes are typically much smaller than optical cavities, which means that the confined space within plasmonic cavities enables strong coupling with individual molecules. This leads to a regime where the interaction between the plasmonic field and a single molecule becomes the dominant factor.⁹ The plasmonic nanocavity mode is a standing wave where the intensity is confined, in contrast to the SPP mode, which is not localized and propagates along the interface, with its intensity exponentially decaying in the direction perpendicular to the interface. It has been demonstrated that the plasmonic cavity mode exhibits superior activity compared to the SPP mode.^{10,11}

At the heart of plasmonic nanocavities is the enhancement of electromagnetic fields, often resulting in localized “hot spots” where the field intensity is significantly higher than that of the incident light. This intense field enhancement facilitates both sensing and light-matter interactions. For example, Raman scattering from molecules near the cavity can be significantly amplified, enabling ultrasensitive detection of molecular species. As a result, Surface-Enhanced Raman Spectroscopy (SERS) becomes a powerful tool for biosensing and chemical detection.^{12–15} In the field of chemical sensing, the localized field enhancement can accelerate reactions by lowering activation energies, enabling real-time monitoring of chemical processes with high temporal resolution.^{16–18} This is particularly useful in catalysis, where plasmonic nanocavities can enhance the efficiency of chemical reactions, such as those involved in energy conversion or environmental remediation.¹⁹ Moreover, intense field enhancements are being explored in the realm of quantum optics and nonlinear optics.^{20–22} Plasmonic nanocavities can facilitate enhanced nonlinear interactions at the nanoscale, open-

ing avenues for the development of novel light sources, quantum communication systems, and high-performance optical sensors.

Although plasmonic nanocavities have been extensively studied in the context of light emission,²³ catalysis,¹¹ and sensing,²⁴ their potential to influence the electronic states and dynamics of molecules—especially during nonadiabatic transitions—remains not fully understood. There have been several theoretical studies on photochemical and photophysical processes in plasmonic cavities. For example, Climent and co-workers²⁵ show that plasmonic nanocavities can alter chemical reaction pathways in the plasmonic nanocavities by means of electronic structure calculations. Fregoni and co-workers²⁶ combined a high-level quantum chemical description of molecules with a quantized model of localized surface plasmons to demonstrate how plasmonic nanocavities can manipulate molecular charge density, providing valuable benchmarks to guide the development of molecular polaritonics. Mondal and co-workers²⁷ present a method to estimate radiation-matter coupling, mode volume, mode lifetime, and quality factor for plasmonic cavities of various shapes. Jamshidi and co-workers²⁸ simulate the complex nature of plasmonic nanocavities and their coupling with emitters within the framework of quantum dynamics, emphasizing the significant role that the plasmonic structure plays in the short-time dynamics of the molecules. Theoretical calculations for plasmonic cavities are still relatively scarce because incorporating plasmonic cavities into theoretical studies poses significant challenges. These systems involve light interacting with electronic states, leading to strong light-matter coupling and hybrid states like polaritons. Electron-phonon couplings further contribute to energy dissipation and decoherence. A robust theoretical framework must capture the complex and quantum coupling between these entities. Furthermore, nonadiabatic effects are crucial for accurately describing processes such as energy transfer, relaxation, and chemical reactions within plasmonic cavities.²⁹

In this study, we utilize the Floquet quantum master equation (FQME) and Floquet surface hopping (FSH) methods, developed in previous work,^{30,31} to investigate nonadiabatic

relaxation processes in plasmonic nanocavities. Pyrazine is selected as the molecular system coupled to the cavity due to its widespread use as a model for nonadiabatic dynamics. This is attributed to its closely spaced S_1 ($n \rightarrow \pi^*$) and S_2 ($\pi \rightarrow \pi^*$) states, which exhibit strong coupling via conical intersections (CIs).^{32,33} We find that the plasmonic cavity effectively facilitates both pumping and relaxation processes. While electron transfer between the molecule and the metal surface influences state populations, it does not significantly impact the overall rates of pumping and relaxation dynamics. This is because we consider a weak coupling between the molecule and the metal surface. The results obtained from FQME and FSH are consistent with each other. Due to the high computational cost of FQME, the FSH method offers a more computationally efficient alternative.

2. THEORY

MODEL HAMILTONIAN

The general model Hamiltonian in our study consists of three components: the system part, which incorporates a time-periodic driving term; the bath part; and the system-bath coupling part:

$$\hat{H}(t) = \hat{H}_S(t) + \hat{H}_B + \hat{H}_C \quad (1)$$

$$\hat{H}_S(t) = \hat{H}_{el}(\hat{\mathbf{R}}, t) + U_0(\hat{\mathbf{R}}) + \sum_{\alpha} \frac{\hat{\mathbf{P}}_{\alpha}^2}{2m_{\alpha}} \quad (2)$$

$$\hat{H}_{el}(\hat{\mathbf{R}}, t) = \sum_{i,j=0}^2 \mathcal{H}_{ij}(\hat{\mathbf{R}}) |S_i\rangle\langle S_j| + (\boldsymbol{\mu} \cdot \mathbf{E}(t) |S_0\rangle\langle S_2| + \text{h.c.}) + E_d(\hat{\mathbf{R}}) \hat{d}^{\dagger} \hat{d} \quad (3)$$

$$\hat{H}_B = \sum_k \epsilon_k \hat{c}_k^{\dagger} \hat{c}_k \quad (4)$$

$$\hat{H}_C = \sum_k V_k (\hat{c}_k^{\dagger} \hat{d} + \hat{d}^{\dagger} \hat{c}_k) \quad (5)$$

Here, \hat{H}_S represents the nuclear and electronic degrees of freedom (DOF) of pyrazine under classical light-matter interaction. Specifically, \mathcal{H}_{ij} accounts for the interaction among the ground state (S_0) and excited states (S_1 and S_2) of pyrazine. For pyrazine, the transition dipole moment between S_0 and S_2 states is much larger than that between S_0 and S_1 states. Therefore, we focus exclusively on the transition dipole moment between S_0 and S_2 states, denoted by $\boldsymbol{\mu}$, which interacts with an electromagnetic field of strength E and frequency Ω , expressed as $\mathbf{E}(t) = \mathbf{E} \cos(\Omega t)$. Here, the term $\boldsymbol{\mu} \cdot \mathbf{E} \cos(\Omega t)$ can be expressed as $A \cos(\Omega t)$, representing a time-periodic driving force with an overall strength of A . Therefore, $\hat{H}_S(t) = \hat{H}_S(t + T)$ with the driving period T . Additionally, a radical anion state S_0^- is introduced by adding an electron to the lowest unoccupied molecular orbital (LUMO) of the S_0 state. This is represented using second quantization notation, where \hat{d}^{\dagger} (\hat{d}) denote the creation (annihilation) operators for the effective spin-up electronic orbital in the LUMO (as shown in the electronic configuration in Figure S1). The term ‘‘effective spin-up electronic orbital’’

is used because we assume that the energy of this orbital (E_d) is equal to the energy difference between the radical anion state and the ground state of pyrazine. Simply considering the addition of an electron to the LUMO is insufficient to achieve the stable pyrazine anion. Under the consideration of the S_0^- state, the \hat{H}_{el} has the matrix form:

$$\hat{H}_{el}(\hat{\mathbf{R}}, t) = \begin{pmatrix} h_0^- & 0 & 0 & 0 \\ 0 & h_0 & 0 & \boldsymbol{\mu} \cdot \mathbf{E}(t) \\ 0 & 0 & h_1 & \lambda Q_c \\ 0 & \boldsymbol{\mu} \cdot \mathbf{E}(t) & \lambda Q_c & h_2 \end{pmatrix} \quad (6)$$

where h_0^- , h_0 , h_1 and h_2 are relative energy of S_0^- , S_0 , S_1 , and S_2 states of the pyrazine with respect to the Fermi level of the metal surface. The energy differences among these four electronic states are given by $h_0^- - h_0 = E_d = E_0 + \kappa_0 Q_t$, $h_1 - h_0 = E_1 + \kappa_1 Q_t$ and $h_2 - h_0 = E_2 + \kappa_2 Q_t$, where $E_0 + \kappa_0 Q_t$ is the effective LUMO energy, E_1 and E_2 are vertical excited energies at the Franck-Condon point. The parameters κ_i ($i = 1, 2$) represent intrastate electron-vibrational coupling constants. In this study, we set $h_0^- = 0$, assuming that the Fermi level is energetically aligned with anion state of pyrazine. Actually, fermi level of the metal can be modulated by surface coating,³⁴ doping,³⁵ interfacial dipole engineering³⁶ and so on. λ is the $S_1 - S_2$ vibronic-coupling constant. The numerical values of the parameters for the system part Hamiltonian in Eq. 2 are taken from Ref. 37: $\hbar\omega_c = 118meV$, $\hbar\omega_t = 74meV$, $\kappa_1 = -105meV$, $\kappa_2 = 149meV$, $\lambda = 261.6meV$, $E_1 = 3.94eV$, $E_2 = 4.84eV$.

The nuclear positions and momenta are represented by $\hat{\mathbf{R}}$ and $\hat{\mathbf{P}}$, with α indexing the nuclear DOF. The nuclear mass is denoted by m_α , and $U_0(\hat{\mathbf{R}})$ represents the diabatic nuclear potential corresponding to the unoccupied electronic state. In this study, we consider three-state two-mode model of pyrazine for the system part, such that

$$U_0(\hat{\mathbf{R}}) = \sum_{\sigma} \frac{1}{2} \hbar\omega_{\sigma} Q_{\sigma}^2 \quad (7)$$

where ω_σ ($\sigma = t$ means tuning mode, $\sigma = c$ means coupling mode) are nuclear oscillation frequencies.

The plasmonic nanocavity's metal states are modeled as a bath Hamiltonian \hat{H}_B , with \hat{c}_k^+ (\hat{c}_k) denotes the creation (annihilation) operator for the k -th electronic orbital of the metal bath. The coupling between the effective molecular orbital \hat{d} and the metallic orbital \hat{c}_k is given by V_k . Under the wide-band approximation, the hybridization function $\Gamma(\epsilon)$, which measures the strength of the system-bath coupling, is assumed to be independent of ϵ and is expressed as:

$$\Gamma(\epsilon) = 2\pi \sum_k |V_k|^2 \delta(\epsilon - \epsilon_k) = \Gamma \quad (8)$$

Taking into account the light-matter interaction in a plasmonic nanocavity, the Hamiltonian becomes time-periodic. Here, we apply Floquet theory to convert the time-periodic Hamiltonian into a time-independent representation within Floquet space.³⁸ As introduced in previous works,³⁹ to construct time-independent Floquet Hamiltonian \hat{H}^F , we define two key operators: the Fourier number operator \hat{N} and the Fourier ladder operators \hat{L}_n . These operators exhibit the following properties:

$$\hat{N} |n\rangle = n |n\rangle, \hat{L}_n |m\rangle = |n + m\rangle \quad (9)$$

where $|n\rangle$ is the basis set in the Fourier space. Then the Hamiltonian and density operator in Floquet representation would be

$$\hat{H}^F = \sum_n \hat{H}^{(n)} \hat{L}_n + \hat{N} \hbar \Omega \quad (10)$$

$$\hat{\rho}^F(t) = \sum_n \hat{\rho}^{(n)}(t) \hat{L}_n \quad (11)$$

Here, $\hat{H}^{(n)}$ and $\hat{\rho}^{(n)}(t)$ represent the Fourier expansion coefficients in the expansions $\hat{H}(t) = \sum_n \hat{H}^{(n)} e^{in\omega t}$ and $\hat{\rho}(t) = \sum_n \hat{\rho}^{(n)}(t) e^{in\omega t}$, respectively, where n is an integer ranges from $-\infty$ to ∞ . In practical calculation, the value of n must be truncated based on the ratio of the

driving amplitude and the driving frequency, $\frac{A}{\hbar\Omega}$. A smaller ratio of $\frac{A}{\hbar\Omega}$ requires a smaller n to achieve convergence in the calculation. By applying Floquet theory, the Hamiltonian is transformed into a time-independent form; however, this comes at the cost of enlarging the Hamiltonian matrix. In the Floquet representation, considering the smallest case, the system will have three Floquet levels ($n = \pm 1, 0$), meaning the original Hamiltonian will expand to three times its original size.

Floquet Quantum Master Equation (FQME)

We can demonstrate that Liouville-von Neumann (LvN) equation still hold in Floquet representation as:^{39,40}

$$\frac{\partial}{\partial t}\hat{\rho}^F(t) = -\frac{i}{\hbar}[\hat{H}^F, \hat{\rho}^F(t)] \quad (12)$$

Correspondingly, the Redfield equation for the molecule density operator in Floquet representation, $\hat{\rho}_S^F(t)$ reads as

$$\frac{\partial}{\partial t}\hat{\rho}_S^F(t) = -\frac{i}{\hbar}[\hat{H}_S^F, \hat{\rho}_S^F(t)] - \hat{\mathcal{L}}_{BS}^F\hat{\rho}_S^F(t) \quad (13)$$

We refer to Eq. (13) as the Floquet quantum master equation(FQME). Here, $\hat{\mathcal{L}}_{BS}^F$ is the Redfield operator. In diabatic representation, the Redfield operator can be expressed as:

$$\begin{aligned} \hat{\mathcal{L}}_{BS}^F\hat{\rho}_S^F &= \frac{\Gamma}{2\hbar}\hat{d}^{F\dagger}\hat{U}\tilde{\mathbb{D}}^F\hat{U}^\dagger\hat{\rho}_S^F(t) \\ &\quad + \frac{\Gamma}{2\hbar}\hat{d}^F\hat{U}\mathbb{D}^{F\dagger}\hat{U}^\dagger\hat{\rho}_S^F(t) \\ &\quad - \frac{\Gamma}{2\hbar}\hat{d}^{F\dagger}\hat{\rho}_S^F(t)\hat{U}\mathbb{D}^F\hat{U}^\dagger \\ &\quad - \frac{\Gamma}{2\hbar}\hat{d}^F\hat{\rho}_S^F(t)\hat{U}\tilde{\mathbb{D}}^{F\dagger}\hat{U}^\dagger + \text{h.c.} \end{aligned} \quad (14)$$

here, $(\mathbb{D}^F)_{NM} \equiv (\hat{U}^\dagger\hat{d}^F\hat{U})_{NM}f(\tilde{E}_N - \tilde{E}_M)$, $(\mathbb{D}^{F\dagger})_{NM} \equiv (\hat{U}^\dagger\hat{d}^{F\dagger}\hat{U})_{NM}f(\tilde{E}_N - \tilde{E}_M)$, $(\tilde{\mathbb{D}}^F)_{NM} \equiv (\hat{U}^\dagger\hat{d}^F\hat{U})_{NM}(1 - f(\tilde{E}_N - \tilde{E}_M))$, $(\tilde{\mathbb{D}}^{F\dagger})_{NM} \equiv (\hat{U}^\dagger\hat{d}^{F\dagger}\hat{U})_{NM}(1 - f(\tilde{E}_N - \tilde{E}_M))$, where \hat{U} and \tilde{E}_N are the eigenvectors and eigenvalues of the Floquet system Hamiltonian \hat{H}_S^F , respectively.

$f(E) = 1/(e^{E/(kT)} + 1)$ is the Fermi function. To solve the FQME, we choose 20 harmonic oscillator basis sets for each nuclear vibration mode.

Floquet Surface Hopping (FSH)

Surface hopping is a hybrid method that combines classical and quantum mechanics to model molecular dynamics. In this approach, the nuclear motion is treated classically, meaning that the nuclei follow trajectories based on Newtonian mechanics, and their positions and velocities are updated at each time step. However, the electronic degrees of freedom are treated quantum mechanically, with the system being assumed to be on one of several electronic potential energy surfaces (PESs) at any given moment. To derive surface hopping algorithm, we first perform a partial Wigner transform for Eq. 13 to approximate the nuclear motion classically. Then we arrive at a Floquet quantum-classical Liouville equation-classical master equation (FQCLE-CME) (details can be found in Ref. 31):

$$\begin{aligned} \frac{\partial}{\partial t} \hat{\rho}_{sW}^F(\mathbf{R}, \mathbf{P}, t) = & \frac{1}{2} \{ \hat{H}_{sW}^F(\mathbf{R}, \mathbf{P}), \hat{\rho}_{sW}^F \} - \frac{1}{2} \{ \hat{\rho}_{sW}^F, \hat{H}_{sW}^F(\mathbf{R}, \mathbf{P}) \} \\ & - \frac{i}{\hbar} [\hat{H}_{sW}^F, \hat{\rho}_{sW}^F] - \hat{\mathcal{L}}_{bsW}^F(\mathbf{R}) \hat{\rho}_{sW}^F(t) \end{aligned} \quad (15)$$

here, $\{\cdot, \cdot\}$ is the Poisson bracket,

$$\{A, B\} = \sum_{\alpha} \left(\frac{\partial A}{\partial R_{\alpha}} \frac{\partial B}{\partial P_{\alpha}} - \frac{\partial A}{\partial P_{\alpha}} \frac{\partial B}{\partial R_{\alpha}} \right) \quad (16)$$

and $\hat{H}_{sW}^F(\mathbf{R}, \mathbf{P})$ indicates the partial Wigner transformation of \hat{H}_s^F . Here, $\hat{\mathcal{L}}_{bsW}^F(\mathbf{R})$ becomes position-dependent due to the position-dependent eigenvectors and eigenvalues of $\hat{H}_{sW}^F(\mathbf{R}, \mathbf{P})$. Typically, surface hopping is performed within the adiabatic representation.

Therefore, we need FQCLE-CME in adiabatic representation:

$$\begin{aligned}
\frac{\partial}{\partial t} \rho_{NM}^{F(ad,sW)}(\mathbf{R}, \mathbf{P}, t) = & -\frac{i}{\hbar} (\tilde{E}_N^{ad}(\mathbf{R}) - \tilde{E}_M^{ad}(\mathbf{R})) \rho_{NM}^{F(ad,sW)} \\
& - \sum_{\alpha K} \frac{P_\alpha}{m_\alpha} \left(d_{NK}^\alpha(\mathbf{R}) \rho_{KM}^{F(ad,sW)} - \rho_{NK}^{F(ad,sW)} d_{KM}^\alpha(\mathbf{R}) \right) \\
& - \frac{1}{2} \sum_{\alpha K} \left(F_{NK}^\alpha(\mathbf{R}) \frac{\partial \rho_{KM}^{F(ad,sW)}}{\partial P_\alpha} + \frac{\partial \rho_{NK}^{F(ad,sW)}}{\partial P_\alpha} F_{KM}^\alpha(\mathbf{R}) \right) \\
& - \sum_{\alpha} \frac{P_\alpha}{m_\alpha} \frac{\partial \rho_{NM}^{F(ad,sW)}}{\partial R_\alpha} - \sum_{KL} \mathcal{L}_{NM,KL}^{F(ad,bsW)}(\mathbf{R}) \rho_{KL}^{F(ad,sW)}
\end{aligned} \tag{17}$$

Here, F^α and d^α are the force and the derivative coupling. This FQCLE-CME can be solved by Floquet surface hopping (FSH) algorithm by evolving electronic and nuclear part according to:

$$\begin{aligned}
\dot{\sigma}_{NM}^{F(ad)} = & -\frac{i}{\hbar} (\tilde{E}_N^{ad}(\mathbf{R}) - \tilde{E}_M^{ad}(\mathbf{R})) \sigma_{NM}^{F(ad)} \\
& - \sum_{\alpha K} \frac{P_\alpha}{m_\alpha} \left(d_{NK}^\alpha(\mathbf{R}) \sigma_{KM}^{F(ad)} - \sigma_{NK}^{F(ad)} d_{KM}^\alpha(\mathbf{R}) \right) \\
& - \sum_{KL} \mathcal{L}_{NM,KL}^{F(ad,bsW)}(\mathbf{R}) \sigma_{KL}^{F(ad)}
\end{aligned} \tag{18}$$

$$\dot{R}_\alpha = \frac{P_\alpha}{m_\alpha} \tag{19}$$

$$\dot{P}_\alpha = F_{\alpha(\lambda\lambda)} \tag{20}$$

The hopping rates have two parts: one is caused by the derivative coupling ($k_{N \rightarrow M}^D$), the other one is caused by the interaction between the molecule and the metal surface ($k_{N \rightarrow M}^{\mathcal{L}}$):

$$k_{N \rightarrow M}^D = \Theta \left(-2Re \sum_{\alpha} \frac{P_\alpha}{m_\alpha} \frac{d_{MN}^\alpha \sigma_{NM}^{F(ad)}}{\sigma_{NN}^{F(ad)}} \right) \tag{21}$$

where Θ function is defined as

$$\Theta(x) = \begin{cases} x, & (x \geq 0) \\ 0, & (x < 0) \end{cases} \quad (22)$$

$$k_{N \rightarrow M}^{\mathcal{L}} = -\mathcal{L}_{MM,NN}^{F(ad,bsW)} \quad (23)$$

where we employ the secular approximation to ignore the off-diagonal part of \mathcal{L} , which is accurate in long time dynamics.⁴¹ The details of operating such FSH algorithm step by step are given in Ref. 31.

3. RESULTS AND DISCUSSION

In the present study, we model the potential energy surface (PES) of the pyrazine anion state S_0^- based on experimental results. Experiments indicate that the radical anion of pyrazine is generally more stable than the neutral pyrazine molecule, owing to its π -system. The delocalized π -system in pyrazine allows for the spreading of the additional electron over the ring.⁴²⁻⁴⁴ Moreover, SERS data suggest that the PES of S_0^- shift in the same direction as the S_2 state relative to the ground state along the tuning mode, but to a lesser extent.⁴⁵ Accordingly, we define $\bar{E} = \frac{\kappa_0^2}{2\hbar\omega_t} + E_0$ as the energy difference between the minimum of S_0^- and S_0 states, and set it to be negative. And also we choose κ_0 to have the same sign as κ_2 but with a smaller absolute value than κ_2 . Here, we define two distinct sets of PES parameters to represent two different levels of stability for the pyrazine anion. These diabatic PESs are shown in Figure 1. The pyrazine anion is more stable in PES-2 of the Figure 1 since the absolute value of \bar{E} is larger. In the following, we perform dynamics based on these two PESs. For the $S_2 \rightarrow S_1/S_0/S_0^-$ processes, we prepare the molecule at electronic state S_2 , assuming it is excited vertically from the minimum of the S_0 state. For the $S_0 \rightarrow S_0^-/S_1/S_2$ processes, we prepare the molecule at the minimum of the S_0 state. The molecule is then either pumped to the S_2 state due to the driving force, or transferred to the S_0^- state due to the electron transfer from the metal surface.

$S_2 \rightarrow S_1/S_0/S_0^-$ PROCESSES

First, we consider the scenario where no electron transfer occurs between the molecule and the metal surface, with the molecule initialized on the S_2 state. In this case, the S_0^- state will not be occupied. When the molecule is outside the plasmonic cavity, where no external driving force acts on the molecule, the electronic state population dynamics are depicted in Figure 2a. The electronic excitation relaxes to the S_1 state within 30 *fs* due to the conical intersection (CI) and the strong electron-nuclear coupling.⁴⁶ When the molecule is inside the

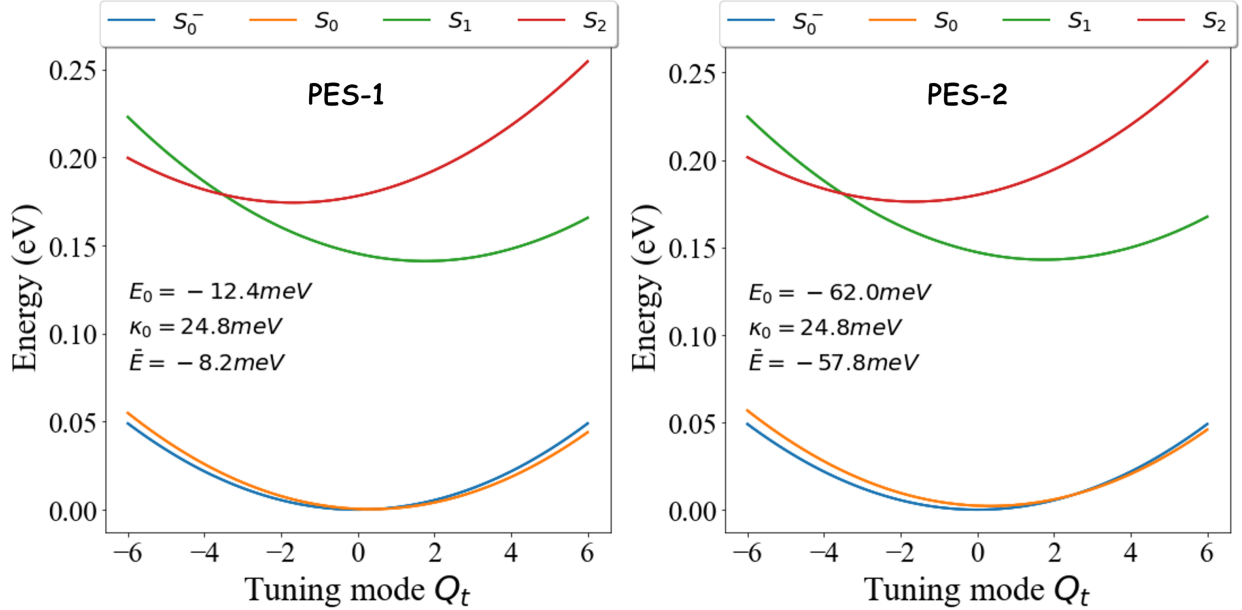


Figure 1: Diabatic potential energy surfaces (PESs) of the S_0^- , S_0 , S_1 , and S_2 states along the tuning mode Q_t . The anion of pyrazine is more stable in PES-2 of right panel.

plasmonic nanocavity, the electromagnetic field couples with the transition dipole moment between S_0 and S_2 states, facilitating electronic state population transfer between these two states. Here, we apply a resonant driving force, with the driving frequency matching the energy difference between the S_2 and S_0 states ($\hbar\Omega = \Delta E_{02}$). Under these conditions, there are two possible channels for the relaxation of electronic excitation from the S_2 state ($S_2 \rightarrow S_1$ and $S_2 \rightarrow S_0$), leading to a faster relaxation dynamics in the S_2 state (within 25 fs), as illustrated in Figure 2b. As the driving strength A increases, populations in the S_2 state relax to both S_0 and S_1 states within 15 fs, as shown in Figure 2c. At early times, the population in the S_0 state is significantly larger than that in the S_1 state due to the strong driving force. Moreover, the oscillation of populations between S_0 and S_2 states are observed, driven by the intense external field. It is noteworthy that the FQME and FSH methods agree closely with each other.

The rapid relaxation caused by the driving forces can also be understood in terms of nuclear dynamics. Figure S2 illustrates the nuclear dynamics along the tuning mode under different driving conditions, assuming no electron transfer between the molecule and the

metal surface. Outside the cavity, the nuclei pass through the CI. However, inside the cavity, the electron can relax via the avoided crossing point induced by the driving, as shown in the Floquet PES in Figure S3. In the Floquet PES, the original PES for each state is expanded into multiple Floquet replicas according to Eq. 10, with the energy difference between each adjacent Floquet replicas corresponding to the driving frequency. Avoided crossings occur between Floquet replicas of S_0 and S_2 states in the adiabatic representation. As a result, during the relaxation processes, the nuclear motion along the tuning mode can also pass through avoided crossing points, and does not necessarily need to reach the CI.

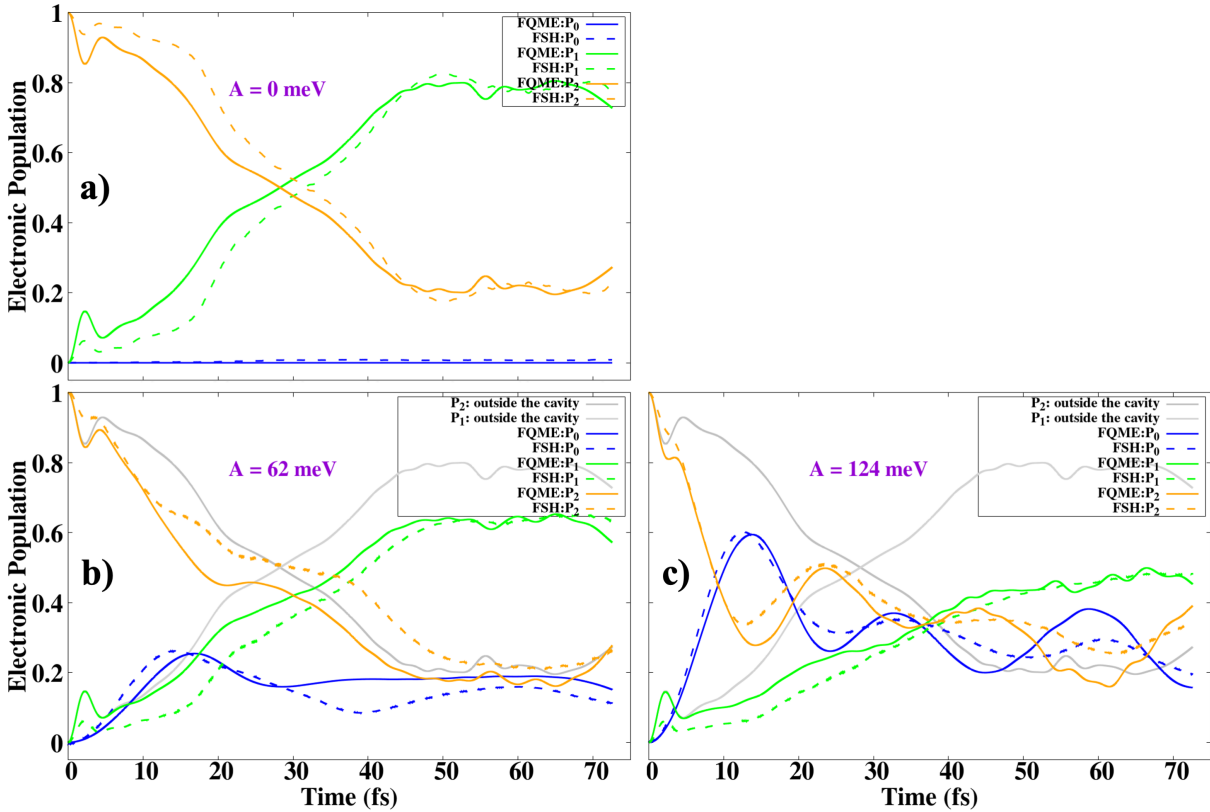


Figure 2: Population dynamics of S_0 , S_1 , and S_2 states under varying driving conditions, in the absence of electron transfer between the molecule and the metal surface ($\Gamma = 0\text{meV}$). The molecule is prepared in the S_2 state. The solid line represents the FQME results, while the dashed line corresponds to the FSH results. We set a resonant driving frequency of $\hbar\Omega = \Delta E_{02}$. a) The driving amplitude $A = 0\text{meV}$, b) the driving amplitude $A = 62\text{meV}$, and c) the driving amplitude $A = 124\text{meV}$. We observe good agreement between FQME and FSH, and the electronic relaxation on S_2 state speeds up as the driving amplitude increases. We observe good agreement between the FQME and FSH results.

Next, we consider the scenario where electron transfer occurs between the molecule and the metal surface as shown in Figure 3. Here, we set a weak coupling between the molecule and the metal surface as $\Gamma = 12.4meV$. In Figure 3, we show the electronic states population dynamics when adding a weak driving of $A = 62meV$. In this case, S_0^- state begins to populate as a function of time. Comparing with Figure 2b, we find that 1) the population of the S_0 decreases, because the system gains electrons from metal surface when it is in the S_0 state, leading to a transition to the S_0^- state; 2) The population of the S_1 decreases because the molecule tends to decay nonadiabatically through avoided crossing points to the S_0 state; 3) The population of the S_0^- state increases more rapidly with time in Figure 3b than in Figure 3a, indicating that the electron transfer rate between the molecule and the metal surface is higher on PES-2, where the S_0^- state is more stable; 4) The electron transfer between the molecule and the metal surface does not affect the relaxation rate. Figure 4 shows the population dynamics when a stronger driving of $A = 124meV$ is applied. Comparing this with Figure 2c, we observe similar changes in the dynamics as seen with the weaker driving field. Additionally, under the influence of a stronger external field, the population of the S_0^- state increases more rapidly over time compared to Figure 3. This is because the population of the S_0^- state is influenced not only by the coupling strength between the molecule and the metal surface, but also by the population of the S_0 state. Stronger fields accelerate the population of the S_0 state, leading to a larger population. This, in turn, enhances electron transfer processes between the molecule and the metal surface under these conditions. We observe good agreement between the FQME and FSH results in Figures 3 and 4.

In this section, we investigate the population dynamics of a molecule initialized in the S_2 state under various driving conditions, considering both cases of electron transfer and no electron transfer between the molecule and the metal surface. We observe that 1) the plasmonic cavity effectively accelerates relaxation from the S_2 state and enhances electron transfer between the molecule and the metal surface; 2) the electron transfer processes affect

the state populations but do not further impact the overall relaxation dynamics rate beyond the effect of the driving.

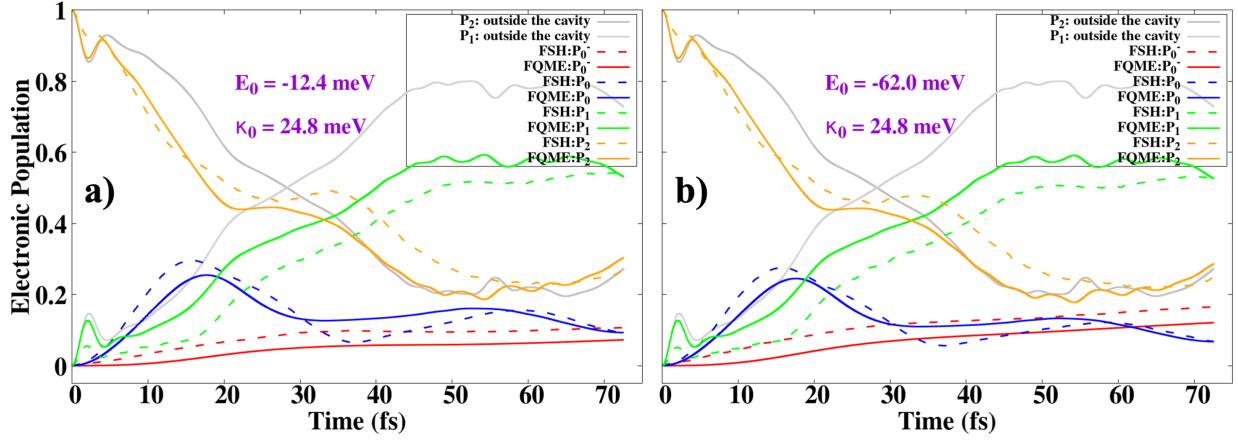


Figure 3: Population dynamics of S_0^- , S_0 , S_1 , and S_2 states under a weak driving force of $A = 62\text{meV}$. The molecule is prepared in the S_2 state. We consider two different PESs of S_0^- , each characterized by different values of E_0 and κ_0 (see Figure 1). We set a weak molecule-metal coupling of $\Gamma = 12.4\text{meV}$. The solid line represents the FQME results, while the dashed line corresponds to the FSH results. We set a resonant driving frequency of $\hbar\Omega = \Delta E_{02}$. Electronic dynamics a) on PES-1, and b) on PES-2. We observe good agreement between the FQME and FSH results.

$S_0 \rightarrow S_0^-/S_1/S_2$ PROCESSES

For these processes, we firstly consider the scenario where no electron transfer occurs between the molecule and the metal surface, with the molecule prepared in the S_0 state. In this case, a driving force must be applied to the system, otherwise, the molecule will remain in the S_0 state. When a weaker driving force is applied, the molecule is first pumped to the S_2 state, and then relaxes to the S_1 state from the S_2 , as shown in Figure 5a. When a stronger driving force is applied, the molecule populates the S_2 state more rapidly and to a greater extent, as shown in Figure 5b. Moreover, the relaxation from the S_2 state is faster under the stronger driving force.

Next, we consider the scenario in which electron transfer takes place between the molecule and the metal surface, and we consider a weak driving force, as depicted in Figure 6. In

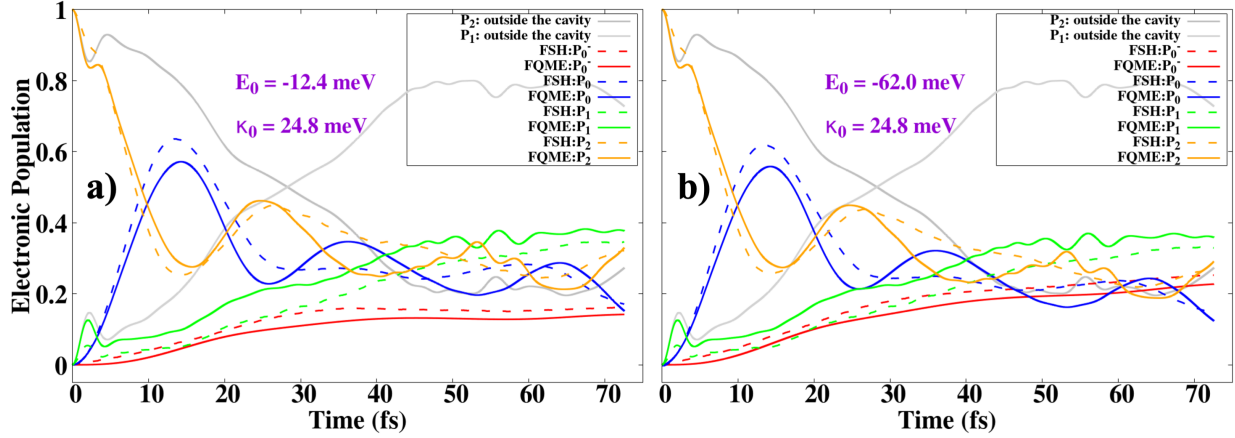


Figure 4: Population dynamics of S_0^- , S_0 , S_1 , and S_2 states under a strong driving force of $A = 124 meV$. The molecule is prepared in the S_2 state. We consider two different PESs of S_0^- , each characterized by different values of E_0 and κ_0 (see Figure 1). We set a weak molecule-metal coupling of $\Gamma = 12.4 meV$. The solid line represents the FQME results, while the dashed line corresponds to the FSH results. We set a resonant driving frequency of $\hbar\Omega = \Delta E_{02}$. Electronic dynamics a) on PES-1, and b) on PES-2. We observe good agreement between the FQME and FSH results.

this case, molecules in the S_0 state can be either transferred to the S_2 state, or to the S_0^- state at early times. As a result, compared to Figure 5a, the population in the S_2 state decreases, while the population in the S_0^- increases. In Figure 6b, the population of the S_0^- state increases more rapidly than in Figure 6a, indicating a faster electron transfer between the molecule and the metal surface. This is because the S_0^- state is more stable under PES-2 condition. When a strong driving force is applied on the system, the population of the S_0^- state also increases, as shown in Figure 7. However, the increase is less pronounced than with a weak driving force. This is because the strong driving force facilitates the transition from the S_0 state to the S_2 state. Since the coupling between the molecule and the metal surface is weak, the electron transfer processes occur much more slowly than the pumping process. Note that when the molecules are initially prepared in the S_0 state, the driving effect on electron transfer processes differs from that observed when they are prepared in the S_2 state. This is because electron transfer processes are influenced by the population of the S_0 state.

In this section, we investigate the population dynamics of a molecule initialized in the S_0 state, examining both scenarios with and without electron transfer between the molecule and the metal surface under different driving conditions. We observe that 1) the plasmonic cavity effectively facilitates both pumping and relaxation processes; 2) while electron transfer processes influence state populations, they do not further impact the overall rates of pumping and relaxation dynamics beyond the effect of the driving.

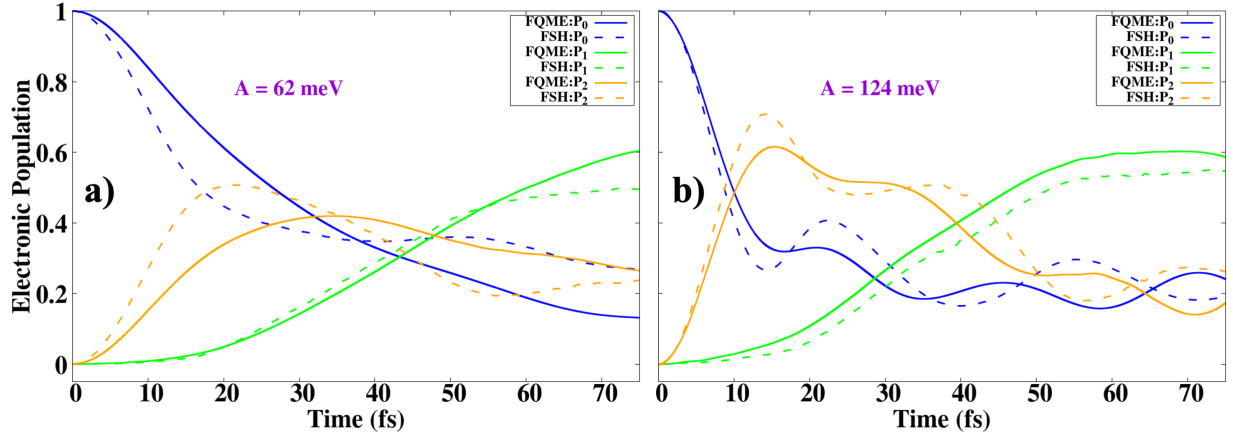


Figure 5: Population dynamics of S_0 , S_1 , and S_2 states under varying driving conditions, in the absence of electron transfer between the molecule and the metal surface ($\Gamma = 0\text{meV}$). The molecule is prepared in the S_0 state. The solid line represents the FQME results, while the dashed line corresponds to the FSH results. We set a resonant driving frequency of $\hbar\Omega = \Delta E_{02}$. a) the driving amplitude $A = 62\text{meV}$, and b) the driving amplitude $A = 124\text{meV}$. We observe good agreement between the FQME and FSH results.

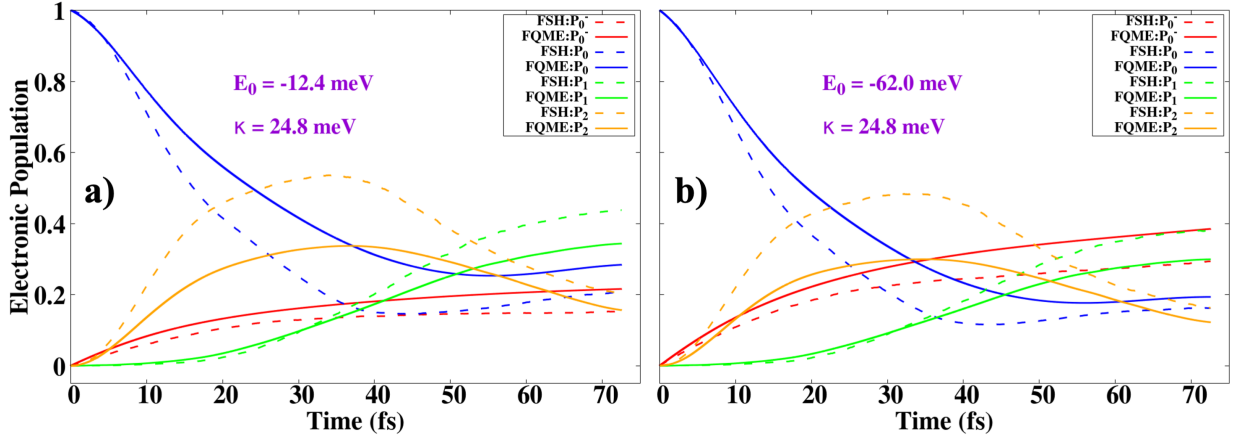


Figure 6: Population dynamics of S_0^- , S_0 , S_1 , and S_2 states under a weak driving force of $A = 62 meV$. The molecule is prepared in the S_0 state. We consider two different PESs of S_0^- , each characterized by different values of E_0 and κ_0 (see Figure 1). We set a weak molecule-metal coupling of $\Gamma = 12.4 meV$. The solid line represents the FQME results, while the dashed line corresponds to the FSH results. We set a resonant driving frequency of $\hbar\Omega = \Delta E_{02}$. Electronic dynamics a) on PES-1, and b) on PES-2. We observe good agreement between the FQME and FSH results.

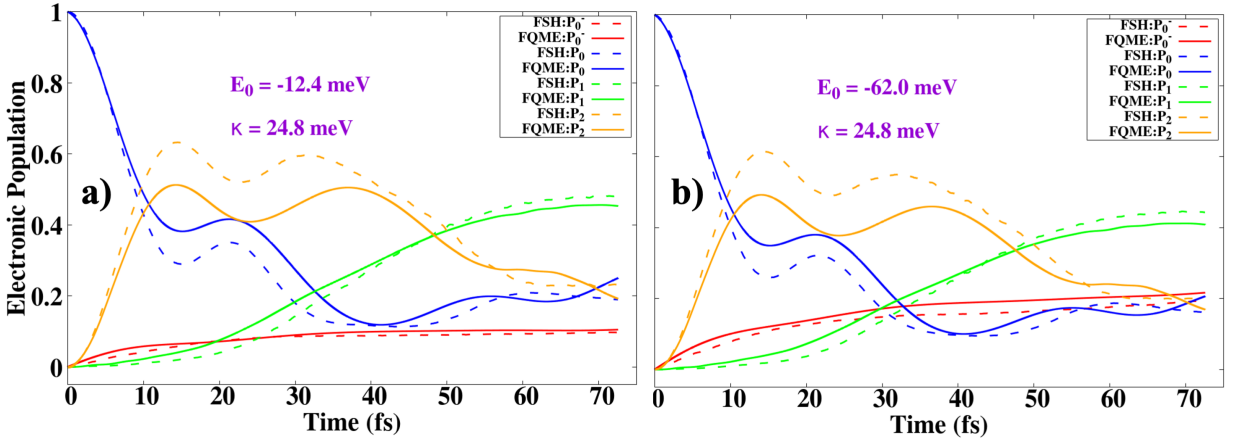


Figure 7: Population dynamics of S_0^- , S_0 , S_1 , and S_2 states under a weak driving force of $A = 124 meV$. The molecule is prepared in the S_0 state. We consider two different PESs of S_0^- , each characterized by different values of E_0 and κ_0 (see Figure 1). We set a weak molecule-metal coupling of $\Gamma = 12.4 meV$. The solid line represents the FQME results, while the dashed line corresponds to the FSH results. We set a resonant driving frequency of $\hbar\Omega = \Delta E_{02}$. Electronic dynamics a) on PES-1, and b) on PES-2. We observe good agreement between the FQME and FSH results.

4. CONCLUSIONS

In this study, we used pyrazine as a model molecule to investigate the influence of plasmonic nanocavities on nonadiabatic dynamics. Our findings reveal that when the molecule is initialized in the S_2 state, the plasmonic cavity effectively accelerates relaxation from the S_2 state and enhances electron transfer between the molecule and the metal surface. Although these electron transfer processes affect the state populations, they do not significantly alter the overall relaxation rate beyond the effect of the external driving field. In contrast, when the molecule is initialized in the S_0 state, the plasmonic cavity facilitates both pumping and relaxation processes. Here, electron transfer processes influence state populations but do not further impact the overall rates of pumping and relaxation beyond the driving effect. These results highlight the role of plasmonic cavities in modulating molecular dynamics, offering insights into how plasmonic interactions can be tailored to control electron and energy transfer in ultrafast processes. FSH method, which is computationally less demanding, agrees well with FQME under all the conditions we considered. Therefore, we can rely on the FSH method for simulating larger systems in the future. Our work opens up new possibilities for designing plasmonic systems that can manipulate both electronic transitions and relaxation dynamics in a variety of applications, from chemical reactions to quantum information processing.

Acknowledgement

D.W. acknowledges supports from the National Natural Science Foundation of China No. 22273075. Y.W. acknowledges supports from the National Natural Science Foundation of China No. 22403077.

References

- (1) Kwon, S.-H.; No, Y.-S.; Park, H.-G. Design of plasmonic cavities. *Nano Convergence* **2014**, *1*, 1–9.
- (2) Hugall, J. T.; Singh, A.; van Hulst, N. F. Plasmonic cavity coupling. *Acs Photonics* **2018**, *5*, 43–53.
- (3) Bitton, O.; Haran, G. Plasmonic cavities and individual quantum emitters in the strong coupling limit. *Accounts of chemical research* **2022**, *55*, 1659–1668.
- (4) Mandal, A.; Taylor, M. A.; Weight, B. M.; Koessler, E. R.; Li, X.; Huo, P. Theoretical advances in polariton chemistry and molecular cavity quantum electrodynamics. *Chemical Reviews* **2023**, *123*, 9786–9879.
- (5) Ditlbacher, H.; Hohenau, A.; Wagner, D.; Kreibig, U.; Rogers, M.; Hofer, F.; Aussenegg, F. R.; Krenn, J. R. Silver nanowires as surface plasmon resonators. *Physical review letters* **2005**, *95*, 257403.
- (6) Kress, S. J.; Antolinez, F. V.; Richner, P.; Jayanti, S. V.; Kim, D. K.; Prins, F.; Riedinger, A.; Fischer, M. P.; Meyer, S.; McPeak, K. M., et al. Wedge waveguides and resonators for quantum plasmonics. *Nano letters* **2015**, *15*, 6267–6275.
- (7) Perney, N.; García de Abajo, F. J.; Baumberg, J.; Tang, A.; Netti, M.; Charlton, M.; Zoorob, M. Tuning localized plasmon cavities for optimized surface-enhanced Raman

- scattering. *Physical Review B—Condensed Matter and Materials Physics* **2007**, *76*, 035426.
- (8) Novotny, L.; Van Hulst, N. Antennas for light. *Nature photonics* **2011**, *5*, 83–90.
- (9) Maccaferri, N.; Barbillon, G.; Koya, A. N.; Lu, G.; Acuna, G. P.; Garoli, D. Recent advances in plasmonic nanocavities for single-molecule spectroscopy. *Nanoscale Advances* **2021**, *3*, 633–642.
- (10) Lyu, P.-T.; Liu, X.-R.; Yin, L.-X.; Wu, P.; Sun, C.; Chen, H.-Y.; Xu, J.-J.; Kang, B. Periodic distributions and ultrafast dynamics of hot electrons in plasmonic resonators. *Nano Letters* **2023**, *23*, 2269–2276.
- (11) Lyu, P.-T.; Yin, L.-X.; Shen, Y.-T.; Gao, Z.; Chen, H.-Y.; Xu, J.-J.; Kang, B. Plasmonic cavity-catalysis by standing hot carrier waves. *Journal of the American Chemical Society* **2023**, *145*, 18912–18919.
- (12) Im, H.; Bantz, K. C.; Lee, S. H.; Johnson, T. W.; Haynes, C. L.; Oh, S.-H. Self-assembled plasmonic nanoring cavity arrays for SERS and LSPR biosensing. *Advanced Materials* **2013**, *25*, 2678–2685.
- (13) Maier, S. A. Plasmonic field enhancement and SERS in the effective mode volume picture. *Optics Express* **2006**, *14*, 1957–1964.
- (14) Li, N.; Feng, L.; Teng, F.; Lu, N. Fabrication of plasmonic cavity arrays for SERS analysis. *Nanotechnology* **2017**, *28*, 185301.
- (15) Sharma, Y.; Dhawan, A. Hybrid nanoparticle–nanoline plasmonic cavities as SERS substrates with gap-controlled enhancements and resonances. *Nanotechnology* **2014**, *25*, 085202.
- (16) Ameling, R.; Langguth, L.; Hentschel, M.; Mesch, M.; Braun, P. V.; Giessen, H. Cavity-enhanced localized plasmon resonance sensing. *Applied Physics Letters* **2010**, *97*.

- (17) Li, C.-Y.; Duan, S.; Yi, J.; Wang, C.; Radjenovic, P. M.; Tian, Z.-Q.; Li, J.-F. Real-time detection of single-molecule reaction by plasmon-enhanced spectroscopy. *Science Advances* **2020**, *6*, eaba6012.
- (18) Kwon, J. A.; Jin, C. M.; Shin, Y.; Kim, H. Y.; Kim, Y.; Kang, T.; Choi, I. Tunable plasmonic cavity for label-free detection of small molecules. *ACS applied materials & interfaces* **2018**, *10*, 13226–13235.
- (19) Fojt, J.; Erhart, P.; Sch" afer, C. Controlling Plasmonic Catalysis via Strong Coupling with Electromagnetic Resonators. *Nano Letters* **2024**, *24*, 11913–11920.
- (20) Marquier, F.; Sauvan, C.; Greffet, J.-J. Revisiting quantum optics with surface plasmons and plasmonic resonators. *ACS photonics* **2017**, *4*, 2091–2101.
- (21) Fryett, T.; Zhan, A.; Majumdar, A. Cavity nonlinear optics with layered materials. *Nanophotonics* **2017**, *7*, 355–370.
- (22) Panoiu, N. C.; Sha, W. E.; Lei, D.; Li, G. Nonlinear optics in plasmonic nanostructures. *Journal of Optics* **2018**, *20*, 083001.
- (23) Russell, K. J.; Liu, T.-L.; Cui, S.; Hu, E. L. Large spontaneous emission enhancement in plasmonic nanocavities. *Nature Photonics* **2012**, *6*, 459–462.
- (24) Butt, M. A. Review of Innovative Cavity Designs in Metal–Insulator–Metal Waveguide-Based Plasmonic Sensors. *Plasmonics* **2024**, 1–20.
- (25) Climent, C.; Galego, J.; Garcia-Vidal, F. J.; Feist, J. Plasmonic Nanocavities Enable Self-Induced Electrostatic Catalysis. *Angewandte Chemie International Edition* **2019**, *58*, 8698–8702.
- (26) Fregoni, J.; Haugland, T. S.; Pipolo, S.; Giovannini, T.; Koch, H.; Corni, S. Strong coupling between localized surface plasmons and molecules by coupled cluster theory. *Nano Letters* **2021**, *21*, 6664–6670.

- (27) Mondal, M.; Semenov, A.; Ochoa, M. A.; Nitzan, A. Strong coupling in infrared plasmonic cavities. *The Journal of Physical Chemistry Letters* **2022**, *13*, 9673–9678.
- (28) Jamshidi, Z.; Kargar, K.; Mendive-Tapia, D.; Vendrell, O. Coupling molecular systems with plasmonic nanocavities: A quantum dynamics approach. *The Journal of Physical Chemistry Letters* **2023**, *14*, 11367–11375.
- (29) Fregoni, J.; Garcia-Vidal, F. J.; Feist, J. Theoretical challenges in polaritonic chemistry. *ACS photonics* **2022**, *9*, 1096–1107.
- (30) Wang, Y.; Dou, W. Nonadiabatic dynamics near metal surface with periodic drivings: A Floquet surface hopping algorithm. *The Journal of Chemical Physics* **2023**, *158*.
- (31) Wang, Y.; Mosallanejad, V.; Liu, W.; Dou, W. Nonadiabatic dynamics near metal surfaces with periodic drivings: A generalized surface hopping in Floquet representation. *Journal of Chemical Theory and Computation* **2024**, *20*, 644–650.
- (32) Seidner, L.; Stock, G.; Sobolewski, A.; Domcke, W. A b initio characterization of the S₁–S₂ conical intersection in pyrazine and calculation of spectra. *The Journal of chemical physics* **1992**, *96*, 5298–5309.
- (33) Woywod, C.; Domcke, W.; Sobolewski, A. L.; Werner, H.-J. Characterization of the S₁–S₂ conical intersection in pyrazine using ab initio multiconfiguration self-consistent-field and multireference configuration-interaction methods. *The Journal of chemical physics* **1994**, *100*, 1400–1413.
- (34) Kim, H. K.; Hyla, A. S.; Winget, P.; Li, H.; Wyss, C. M.; Jordan, A. J.; Larrain, F. A.; Sadighi, J. P.; Fuentes-Hernandez, C.; Kippelen, B., et al. Reduction of the work function of gold by N-heterocyclic carbenes. *Chemistry of Materials* **2017**, *29*, 3403–3411.
- (35) Shi, Y.; Kim, K. K.; Reina, A.; Hofmann, M.; Li, L.-J.; Kong, J. Work function engineering of graphene electrode via chemical doping. *ACS nano* **2010**, *4*, 2689–2694.

- (36) Ma, Y.; Gong, J.; Zeng, P.; Liu, M. Recent progress in interfacial dipole engineering for perovskite solar cells. *Nano-Micro Letters* **2023**, *15*, 173.
- (37) Schneider, R.; Domcke, W.; Köppel, H. Aspects of dissipative electronic and vibrational dynamics of strongly vibronically coupled systems. *The Journal of chemical physics* **1990**, *92*, 1045–1061.
- (38) Shirley, J. H. Solution of the Schrödinger equation with a Hamiltonian periodic in time. *Physical Review* **1965**, *138*, B979.
- (39) Mosallanejad, V.; Chen, J.; Dou, W. Floquet-driven frictional effects. *Physical Review B* **2023**, *107*, 184314.
- (40) Leskes, M.; Madhu, P.; Vega, S. Floquet theory in solid-state nuclear magnetic resonance. *Progress in nuclear magnetic resonance spectroscopy* **2010**, *57*, 345–380.
- (41) Dou, W.; Subotnik, J. E. A generalized surface hopping algorithm to model nonadiabatic dynamics near metal surfaces: The case of multiple electronic orbitals. *Journal of chemical theory and computation* **2017**, *13*, 2430–2439.
- (42) Nenner, I.; Schulz, G. Temporary negative ions and electron affinities of benzene and N-heterocyclic molecules: pyridine, pyridazine, pyrimidine, pyrazine, and s-triazine. *The Journal of Chemical Physics* **1975**, *62*, 1747–1758.
- (43) Song, J. K.; Lee, N. K.; Kim, S. K. Photoelectron spectroscopy of pyrazine anion clusters. *The Journal of chemical physics* **2002**, *117*, 1589–1594.
- (44) Palihawadana, P.; Sullivan, J.; Buckman, S.; Brunger, M. Electron scattering from pyrazine: Elastic differential and integral cross sections. *The Journal of Chemical Physics* **2012**, *137*.
- (45) Arenas, J. F.; Woolley, M. S.; Otero, J. C.; Marcos, J. I. Charge-transfer processes in

surface-enhanced Raman scattering. Franck- condon active vibrations of pyrazine. *The Journal of Physical Chemistry* **1996**, *100*, 3199–3206.

- (46) Gu, B.; Mukamel, S. Manipulating nonadiabatic conical intersection dynamics by optical cavities. *Chemical science* **2020**, *11*, 1290–1298.

Supporting Information: Manipulating nonadiabatic dynamics by plasmonic nanocavity

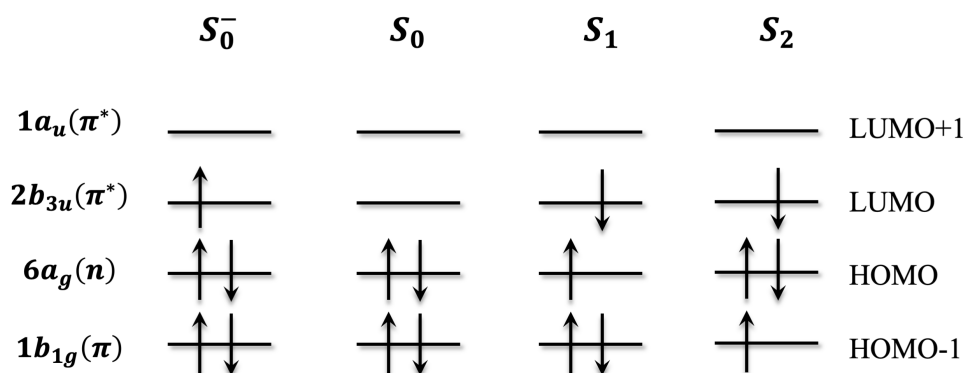


Figure 8: Electronic configurations of S_0^- , S_0 , S_1 and S_2 states. Here, HOMO means the highest occupied molecular orbital, and LUMO means the lowest unoccupied molecular orbital.

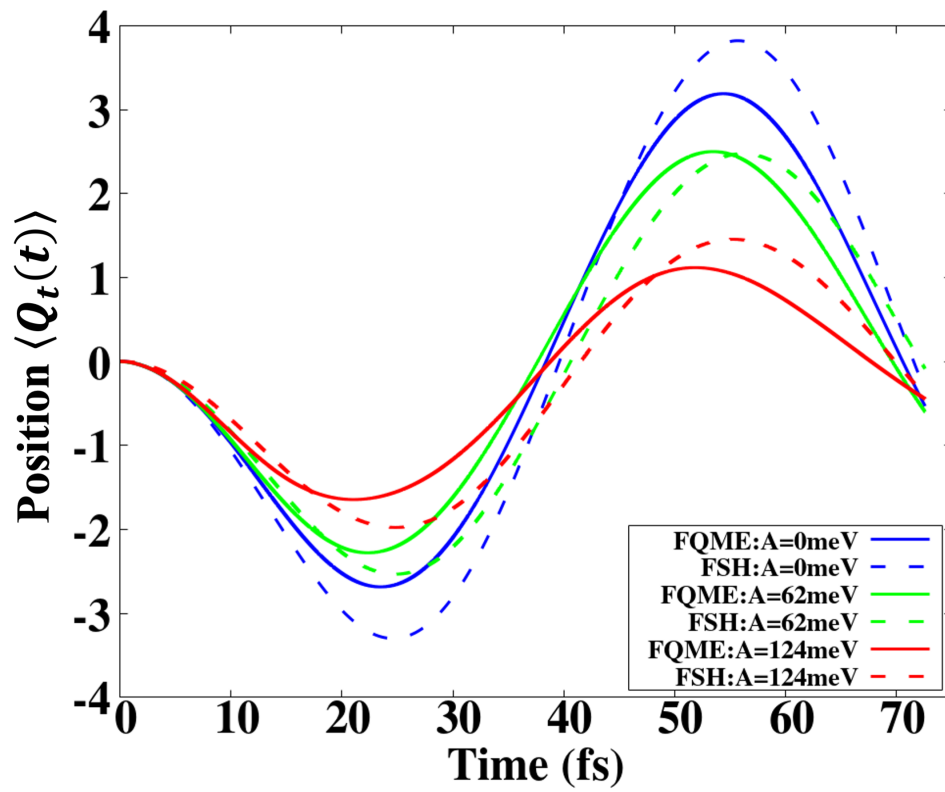


Figure 9: Nuclear dynamics along the tuning mode under different driving conditions.

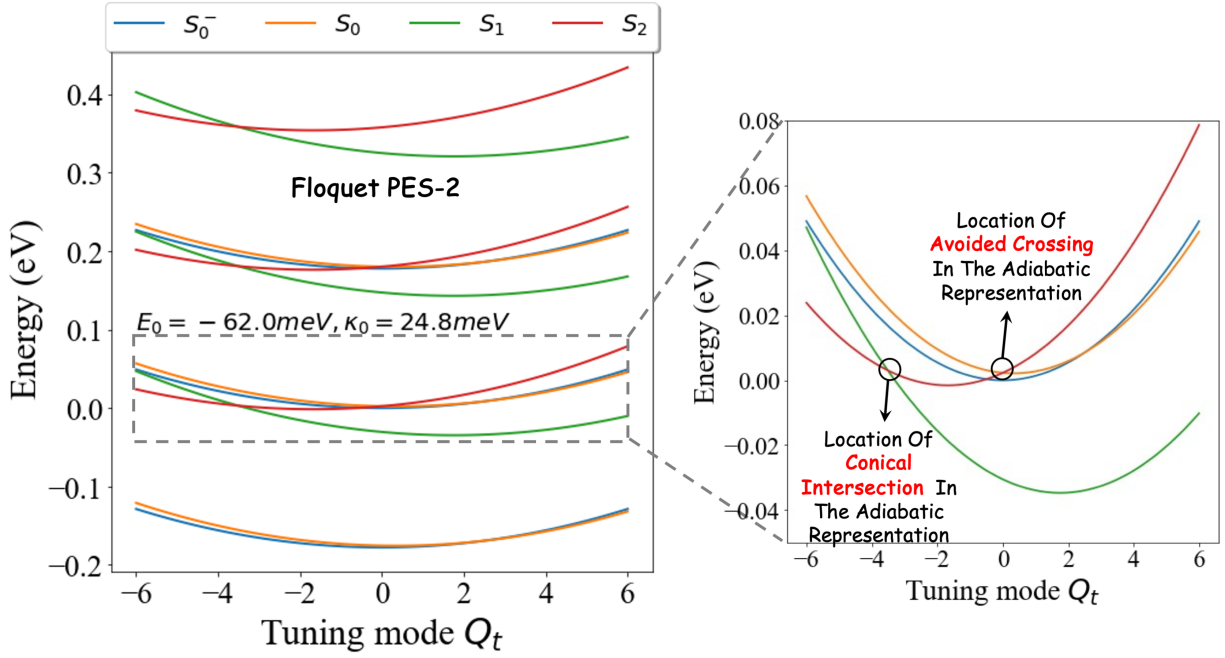


Figure 10: The Floquet diabatic potential energy surfaces of S_0^- , S_0 , S_1 , S_2 states along the tuning mode. Here, we consider three Floquet levels, which means each state has three Floquet replicas with energy difference $\hbar\Omega$. The inset highlights the location of conical intersection in the adiabatic representation due to the coupling between S_2 and S_1 states, as well as the location of avoided crossing in the adiabatic representation due to the coupling between S_2 and S_0 states.